Paleoseismology of the 2010 Mw 7.1 Darfield (Canterbury) earthquake source, Greendale Fault, New Zealand

S. Hornblow
M. Quigley
A. Nicol
R. J. Van Dissen

GNS Science Report 2014/26
June 2014

BIBLIOGRAPHIC REFERENCE

Hornblow, S.; Nicol, A.; Quigley, M.; Van Dissen, R. J. 2014. Paleoseismology of the 2010 M_w 7.1 Darfield (Canterbury) earthquake source, Greendale Fault, New Zealand, *GNS Science Report* 2014/26. 27 p.

S. Hornblow, Department of Geological Sciences, University of Canterbury, Christchurch, New Zealand

A. Nicol, GNS Science, GNS Science, PO Box 30368, Lower Hutt, New Zealand

M. Quigley, Department of Geological Sciences, University of Canterbury, Christchurch, New Zealand

R. J. Van Dissen, GNS Science, GNS Science, PO Box 30368, Lower Hutt, New Zealand

ISSN 1177-2425 (Print)
ISSN 2350-3424 (Online)
ISBN 978-1-927278-50-5

CONTENTS

FIGURES

TABLES

LAYMAN'S ABSTRACT

Rupture of the previously unknown Greendale Fault was the main source of energy release of the large September 2010 Darfield Earthquake, Canterbury, New Zealand. Rupture of the Greendale Fault was large enough to reach the ground surface and it resulted in a deformation zone up to 300 m wide that comprised both concentrated (discrete faulting) and distributed (folding) deformation. Along the central portion of the 2010 ground-surface rupture, discrete surface faulting accommodates ~30% of the total right-lateral displacement; the remainder is accommodated by distributed deformation. Our ability to characterise the width of the surface-rupture deformation zone, and the relative proportions of discrete and distributed deformation, will aid in future land-use planning decisions, and the design of rupture-resilient buildings and lifelines (e.g. pipes and cable networks) on, or across, other active faults in New Zealand and elsewhere.

Shallow subsurface investigations across the Greendale Fault (e.g. trench excavations, and ground penetrating radar), in combination with age dating of these shallow sediments, reveal that the most recent rupture of the Greendale Fault prior to 2010 probably occurred sometime between 20,000 and 30,000 years ago. The knowledge of the amount of time between successive ruptures (large earthquakes) on the Greendale Fault greatly aids in the appropriate application of the Ministry for the Environment's active fault guidelines which are aimed at mitigating the impacts of building on, or near, active faults.

The Greendale Fault remained undetected prior to the Darfield earthquake because evidence of fault rupture at 20,000 to 30,000 years ago had been eroded and buried by younger Waimakariri river gravels. Similar active faults with low rates of movement compared to rates of erosion and sediment accumulation are likely to be concealed near other cities in New Zealand, and elsewhere, within young geological settings similar to Canterbury.

TECHNICAL ABSTRACT

The previously unknown Greendale Fault ruptured in the September 2010 moment magnitude (M_w) 7.1 Darfield Earthquake. Surface rupture fracture patterns and displacements along the fault were measured with high precision using real time kinematic (RTK) GPS, tape and compass, airborne light detection and ranging (LiDAR), and aerial photos. No geomorphic evidence of a penultimate surface rupture was revealed from pre-2010 imagery. The fault zone is up to 300 m wide and comprises both discrete (faulting) and distributed (folding) deformation dominated by right-lateral displacement. Along the central portion of the 2010 ground-surface rupture of the Greendale Fault, discrete surface fracturing accommodates ~30% of the total right-lateral displacement; the remainder is accommodated by distributed deformation. Ground penetrating radar and trenching investigations conducted across the central Greendale Fault reveal that most surface fractures are undetectable at depths ≥ 1 m below the surface; however, large (>5 m long), discrete Riedel shears continue to depths exceeding 3 metres and displace interbedded gravels and thin sand-filled paleo-channels. At one trench site, a Riedel shear displaces surface agricultural markers (e.g., fences, roads and plough lines) and a subsurface (0.6 m deep) paleo-channel by 60 cm right-laterally and 10 cm vertically, indicating that the paleo-channel has been displaced only in the Darfield earthquake. Optically stimulated luminescence (OSL) dating of the paleo-channel yields an age of 21.6 ± 1.5 ka. Two additional paleo-channels at ~2.5 m depth with OSL ages of 28.4 ± 2.4 ka and 33 ± 2 ka have been displaced ~120 cm right-laterally and ~20 cm vertically. The doubling of displacement at depth is interpreted to indicate that in the central section of the Greendale Fault the penultimate surface-rupturing event occurred between ca. 20 and 30 ka.

The one determined inter-event time for the Greendale Fault of 20–30 kyr is compatible with average recurrence intervals that range between ~10 kyr and ~61 kyr, assuming that average recurrence interval has a lognormal distribution and a coefficient of variation of 0.4 to 0.8, and that the minimum and maximum “permissible” average recurrence intervals are, respectively, within plus one standard and minus one standard deviation of the inter-event time. Given the long inter-event time and the implied “permissible” range of average recurrence intervals, we reclassify the Recurrence Interval Class of the Greendale Fault to RIC V (10,000 to 20,000 years), in accord with the Ministry for the Environment’s active fault guidelines, compared to the previous provisional estimation of RIC IV (5000 to 10,000 years).

The Greendale Fault remained undetected prior to the Darfield earthquake because the penultimate fault scarp was eroded and buried during Late Pleistocene alluvial activity on the Waimakariri River fan. Similar active faults with low slip rates (i.e., lower than the rates of sedimentation or erosion) are likely to be concealed in alluvial settings globally.

KEYWORDS

Paleoearthquakes, ground surface rupture, strike slip displacements, Darfield Earthquake, Greendale Fault

1.0 INTRODUCTION

Despite significant scientific advances in the detection and mapping of active faults worldwide, many recent earthquakes have occurred partially, or entirely, on previously unknown faults. These include the 2003 M_w 6.7 Bam (26,000 fatalities) (Fielding et al., 2009), 2008 M_w 7.9 Wenchuan (more than 87,000 fatalities) (Liu-Zeng et al., 2010), 2010 M_w 7.0 Haiti (316,000 fatalities) (Calais et al., 2010), 2010 El Cucapah M_w 7.2, (>100 injured, 4 fatalities) (Oskin et al., 2012), and 2010–2011 Canterbury earthquake sequence, including the 2010 Darfield M_w 7.1 earthquake and 2011 Christchurch earthquake (185 fatalities). Understanding why earthquake sources capable of generating surface ruptures were not previously identified, and how the causative faults behave in time and space, is important for assessing the completeness of seismic hazard models and for understanding the maximum earthquake M_w potential for areas where surface rupturing faults exist but have not been identified (e.g., Stirling et al., 2012).

Depositional environments with particularly high rates of sedimentation or erosion (e.g., alluvial fans and incising or aggrading river systems), present challenges to the detection of active faults. In particular, strike-slip faults with typically low-relief rupture traces and evidence for surface offsets may be obscured by erosion or burial. Under-sampling of active faults at the ground surface is exacerbated when their fault slip rates are low relative to the rates of surface processes (e.g., McCalpin 1996), as is common at the peripheries of active plate boundary zones or within plate interiors. Furthermore, when rupture occurs through thick packages of unconsolidated sediments, the total displacement may be expressed as a combination of discrete surface faulting and broad wavelength folding (Van Dissen et al., 2011; Quigley et al., 2012), with the latter typically difficult to recognise in the geologic record (Rockwell et al., 2002; Bray & Kelson 2006; Wesnousky 2008; Fielding et al., 2009; Oskin et al., 2012; Rockwell & Klinger 2013). For this reason, the use of displaced features to estimate the slip and M_w of paleoearthquakes relies upon the careful documentation of single-event coseismic slip and slip variability from historic earthquakes for which slip and M_w were recorded (e.g., Wells & Coppersmith 1994; Wesnousky 2008). Fault zone maturity can complicate this estimate due to the correlation between established fault length and the ratio of subsurface to surface slip. Discrete surface ruptures typically account for 50–60% of the slip of their subsurface equivalent (Dolan & Haravitch 2014).

The 2010 M_w 7.1 Darfield (Canterbury) event triggered the Canterbury earthquake sequence which, as of February 2014, comprises over 4000 earthquakes of magnitude 3 or greater (http://info.geonet.org.nz/display/home/Aftershocks). In addition to the Darfield earthquake, three earthquakes in the sequence were magnitude 6 or greater, with the 22 February, 2011, M_w 6.3 event causing the greatest damage and loss of life (e.g., Kaiser et al., 2012; Bradley et al., 2014) (Figure 1). Of the faults that accrued slip during the Canterbury earthquake sequence only the Greendale Fault generated ground-surface rupture (Figures 1 and 2A) (Quigley et al., 2010a, 2010b; Beavan et al., 2012; Elliott et al., 2012). The Greendale Fault surface rupture morphology and associated coseismic displacements have been extensively studied using combined field, LiDAR, InSAR, and geodetic techniques (Barrell et al., 2011; Van Dissen et al., 2011; Villamor et al., 2011, 2012; Elliott et al., 2012; Quigley et al., 2012; Duffy et al., 2013; Van Dissen et al., 2013a; Litchfield et al., 2014a). The presence of abandoned river meanders and slip-off terraces has been tentatively interpreted to suggest fault-related pre-2010 Holocene uplift at the western end of the Greendale Fault (Campbell et al., 2012). However, neither interpretation of ortho-photographs predating the Darfield earthquake nor analysis of post-Darfield imagery provides unequivocal evidence that the

Greendale Fault had ruptured the existing ground surface prior to 2010. In the absence of a clear pre-2010 surface trace, sub-surface information is required to constrain the paleoearthquake history of the fault. The paleoseismic history of the Greendale Fault has not been studied prior to this investigation.

This report summarises the tectonic, geologic and geomorphic setting of the Greendale Fault, together with a description of the surface rupture morphology and features displaced along the fault. New Ground Penetrating Radar (GPR) and trenching data from two sites on the central Greendale Fault constrain the subsurface fault geometry and displacements. The timing of the penultimate event has been constrained by new optically stimulated luminescence (OSL) dating of faulted stratigraphic units exposed in the trenches. Our results illuminate some of the challenges of detecting and studying active faults in relatively low strain rate alluvial landscapes, and illustrate how robust paleoseismic information can be obtained by combining subsurface displacement measurements with multi-method high resolution surface displacement measurements.

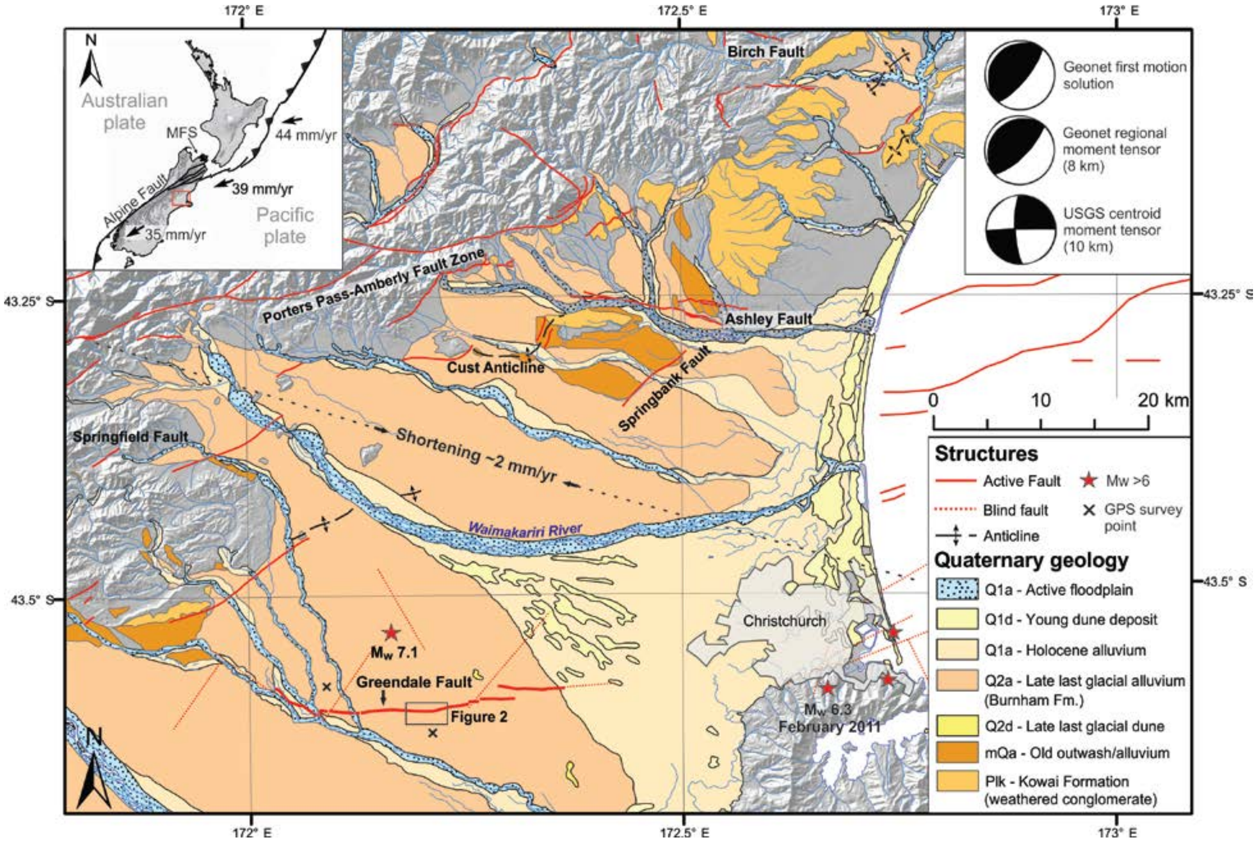

Figure 1 Location map showing active faults (including the Greendale Fault) and Quaternary deposits (modified from Cox & Barrell 2007; Forsyth et al., 2008). Position of blind faults from Beavan et al. (2012). Regional shortening from Wallace et al. (2007). Stars show epicentres of the main events in Canterbury earthquake sequence. Inset (upper left) shows plate boundary setting and relative motion vectors (DeMets et al., 2010). MFS = Marlborough Fault System; location of the study area is shown by the red box. Inset (upper right) shows focal mechanism solutions for the M_w 7.1 September 4 2010 Darfield earthquake.

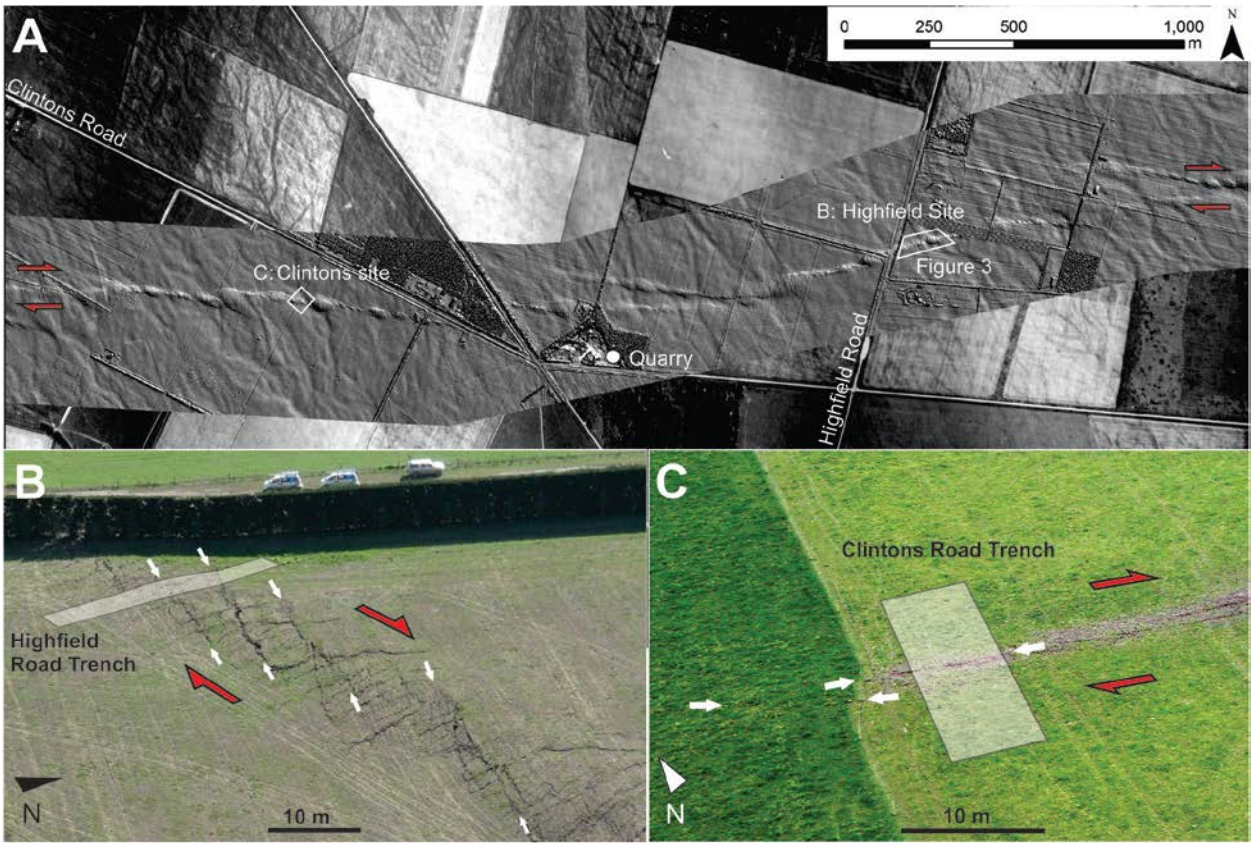

Figure 2 (A) Central Greendale Fault trace geometry shown via post-rupture LiDAR over a 1940s ortho-aerial photo background. The fault trace is highlighted by red arrows and locations of the trench sites are shown. (B) Oblique aerial view of the Highfield Road trench site with Riedel shears highlighted by white arrows. Also visible are antithetic Riedel shears and 'pop-up' structure of fault scarp. Red arrows denote sense of shear. (C) Oblique aerial view of the Clintons Road site with Riedel shears (highlighted by white arrows) offsetting grass verge at the fence line.

2.0 TECTONIC, GEOLOGIC AND GEOMORPHIC SETTING

The Greendale Fault is located in a region of low strain rate at the southeast periphery of the Pacific-Australian plate boundary deformation zone in New Zealand's South Island (Figure 1) (e.g., Wallace et al., 2007). Here, the plates converge in a west to southwest direction at ~35–44 mm/yr, oblique to the boundary structures (e.g., Beavan et al., 2002; Wallace et al., 2007; DeMets et al., 2010). In the central South Island, slip on the Alpine Fault accommodates ~75% of the plate convergence and produces uplift of the Southern Alps, with the remainder of the convergence distributed on faults with lower slip rates, mostly east of the main divide (Norris & Cooper 2001). East of the Southern Alps, in the Canterbury Plains region, few active faults have been mapped at the ground surface (e.g., Cox & Barrell 2007; Forsyth et al., 2008), although geodetic measurements indicate ~2 mm/yr shortening oriented at ~97º east of the Porter's Pass-Amberley fault zone (Figure 1) (Wallace et al., 2007). Some of this shortening may eventually be converted to permanent strain accommodated by anticlines and related thrusts (e.g., Springbank Fault, Springfield Fault and Cust Anticline; for summary see Litchfield et al., 2014b), oriented sub-parallel to the Marlbrough Fault System along the western edge of the Canterbury Plains (Jongens et al., 1999). Prior to the Darfield earthquake it was considered unlikely that these anticlines and thrusts accommodated all of the ~2 mm/yr shortening, and active strike-slip and reverse faults were inferred to be concealed beneath the Canterbury Plains (Pettinga et al., 2001; Wallace et al., 2007) (Figure 1). To account for the possibility of large-magnitude earthquakes on previously unidentified faults a M_w 7.2 maximum cut-off has been used for distributed seismicity in the national seismic hazard model (Stirling & Gerstenberger 2010; Stirling et al., 2012).

The Greendale Fault strikes approximately E-W and is inferred to be a reactivated Cretaceous normal fault (Dorn et al., 2010; Campbell et al., 2012; Davy et al., 2012; Ghisetti & Sibson 2012; Jongens et al., 2012). Seismic reflection profiles on the Canterbury Plains and the offshore Chatham Rise east of Banks Peninsula show many E-W striking normal faults that mainly accrued displacement in the Late Cretaceous to Paleocene (Field et al., 1989; Wood & Herzer 1993; Jongens et al., 1999, 2012; Dorn et al., 2010; Browne et al., 2012; Campbell et al., 2012; Davy et al., 2012; Ghisetti & Sibson 2012). A number of these approximately E-W striking Cretaceous normal faults (e.g., Ashley and Birch faults, Figure 1) have been reactivated in the contemporary stress field (Nicol 1993; Campbell et al., 2012), which has a WNW-ESE (115 ± 5º) trending regional maximum compressive (σ_1) stress (e.g., Nicol & Wise 1992; Balfour et al., 2005; Sibson et al., 2012; Townend et al., 2012). This σ_1 orientation is consistent with predominately right-lateral strike-slip on E-W striking faults, as was produced on the Greendale Fault during the Darfield earthquake (Sibson et al., 2011).

The Darfield earthquake and the Canterbury earthquake sequence occurred within ~30 km thick crust of the Pacific Plate (Eberhart-Philips & Bannister 2002). Basement rocks in Canterbury comprise Permian-Early Cretaceous Torlesse Composite Terrane and their metamorphic equivalents at depth. The majority of the events in the Canterbury earthquake sequence occurred in Torlesse basement and the immediately underlying schists. Beneath the Greendale Fault at a depth of 10–12 km these basement rocks are inferred to rest on Mesozoic ocean crust; the Darfield earthquake may have nucleated close to this boundary between continental and oceanic crust (Reyners et al., 2014). Basement is unconformably overlain by a 1–2.5 km thick cover sequence of Late Cretaceous-Neogene sedimentary and volcanic rocks (Field et al., 1989; Forsyth et al., 2008; Browne et al., 2012). Unconsolidated to weakly lithified Quaternary sediments and sedimentary rocks form a ~240 m to 1 km thick cover underlying the Canterbury Plains (Brown & Weeber 1992; Jongens et al., 1999).

The Greendale Fault displaces the surface of the Canterbury Plains which were formed by a series of coalescing alluvial fans comprising mainly gravels deposited by the river systems draining the Southern Alps (Alloway et al., 2007; Cox & Barrell 2007; Forsyth et al., 2008). These Quaternary gravels are inferred to have been mainly deposited as outwash during periods of glaciation. The latest period of gravel aggradation is thought to have occurred during the Last Glacial Maximum (LGM) (~24,000 to ~18,000 years ago), within the Last Glacial Cold Period (~28,000 to ~18,000 years ago), and waned in response to glacial retreat in the upper reaches of the main river valleys (Alloway et al., 2007; Forsyth et al., 2008). Alluvial aggradation was followed by down-cutting of the main rivers and abandonment of the constructional surface (Cox & Barrell 2007) (Figure 1 and Figure 2). The Greendale Fault ruptured through these alluvial outwash gravels, locally referred to as the Burnham Formation (Forsyth et al., 2008), for ~80% of its length. Exposures of the Burnham Formation indicate that it mainly consists of unconsolidated, moderately well-sorted to very poorly-sorted, moderately- to well-rounded, pebbly to cobbly (clasts <~20 cm) sandy gravels (typically 1–3 m thick), with 10–30 cm thick intercalated lenses of silty sand. Gravel clasts are primarily composed of un-weathered and indurated Torlesse greywacke which, in the region of the central Greendale Fault, were transported southeastwards by the ancestral Waimakariri River.

3.0 GEOMETRY AND SLIP OF THE DARFIELD EARTHQUAKE RUPTURE

InSAR imagery, GPS measurements and seismicity data indicate that the 4 September 2010 M_w 7.1 Darfield earthquake ruptured multiple faults and segments of the same fault. These structures included E-W striking right-lateral, NE-striking reverse, NNW-striking left-lateral, and NW-striking normal right-lateral faults (Beavan et al., 2010, 2012; Holden et al., 2011; Elliott et al., 2012). The modelled maximum slip of >7 m over a 7–8 km strike length occurred at 2–6 km depth, primarily within Torlesse basement rocks, and the combined subsurface rupture length of the three segments of the Greendale Fault is estimated at 48 km (Beavan et al., 2010, 2012). Data from the aftershock sequence following the Greendale Fault rupture show an eastward propagation of seismicity (Bannister & Gledhill 2012) with greatest activity in those areas which did not experience maximum slip during the Darfield earthquake (Syracuse et al., 2013). The inferred upper tip-lines of blind faults (Figure 1) that ruptured in the Darfield earthquake range from 0.5 to 1 km depth (Beavan et al., 2012), suggesting that discrete rupture likely ceased near the base of the Pliocene (~1 km) or Quaternary (~0.5 km) sedimentary deposits (Jongens et al., 2012). Calculation of Darfield earthquake static stress drop for individual segments range from 6 to 10 MPa (Elliott et al., 2012) to 13.9 ± 3.7 MPa averaged over the entire Greendale Fault (Quigley et al., 2012). The larger of these estimates is comparable to the ~16 MPa apparent stress calculated for the Darfield earthquake by Fry & Gerstenberger (2011) and is consistent with failure on a very strong fault.

The Greendale Fault ruptured the ground surface and produced mainly right-lateral displacements across flat grassed farmland (Quigley et al., 2010a, 2010b; Barrell et al., 2011). Mapping of the Greendale Fault at the ground surface took place in the weeks immediately following the earthquake and involved the collection of airborne LiDAR, RTK GPS survey data, and field measurements of vertically and right-laterally displaced features using both tape and compass and RTK (Litchfield et al., 2014a). The intensive agricultural land-use of the Canterbury Plains provided over 100 displaced cultural markers that could be measured with high precision (e.g., roads, fences, crop rows, plough-lines, drains, tree-lines and power-lines).

The 29.5 ± 0.5 km long Greendale Fault surface rupture had a maximum right-lateral surface displacement of 5.3 m (Quigley et al., 2012; Litchfield et al., 2014a). In the central section of the fault, at the ground surface, ~70% of the total right-lateral displacement is accommodated by broad-wavelength (10s to 100s of metres) folding about steeply inclined hinges, and only ~30% is accommodated by discrete (faulting) deformation (Quigley et al., 2010a; Van Dissen et al., 2011, 2013a). Above areas of maximum inferred subsurface slip (~7 m as modelled by Beavan et al., 2012), surface displacements typically range from 4 to 5 m, indicating a vertical decrease in coseismic slip towards the ground surface. This decrease may reflect transfer of slip to wallrock inelastic deformation accommodated by intergranular sliding in unconsolidated gravels. Significant strike-slip gradients were observed along the surface trace across step-overs and where blind faults that slipped during the Darfield event project to intersect the Greendale Fault (Figure 1).

The surface trace of the Greendale Fault is segmented over a range of scales from metres to kilometres. At scales of 100s of metres and less, the surface rupture often comprises a series of en-echelon left-stepping segments separated by pop-up structures which form at restraining steps (e.g., Figure 2A). On the metre to 10s of metres scale, distinctive Riedel (R) and Riedel prime (R′) shears make up the majority of discrete surface deformation and are oriented up to 30º and ~50–70º from the general fault strike, respectively.

4.0 FAULT TRENCHING

Two trench sites, here referred to as Highfield Road (Figure 2B, Figure 3 and Figure 4) and Clintons Road (Figure 2C and Figure 5), characterise the near-surface geometry and paleoearthquake history of the Greendale Fault in its central section. The trenches were excavated in September 2012 (Highfield Road) and March 2013 (Clintons Road), approximately normal to the fault trace to maximum depths of 3–4 m. The trench walls were logged at 1:20 scale and photographed. Stratigraphic units and structures were described and sandy lenses sampled for OSL dating (Table 1). In four instances, paleo-channels, mainly filled with sand or fine gravel, were sequentially excavated along the fault strike to record the horizontal and vertical displacements across Riedel shears.

The surface and sub-surface structure of the fault zone at Highfield Road was also examined using a terrestrial LiDAR survey and GPR, respectively. The terrestrial LiDAR survey was undertaken immediately following the earthquake and records ground fractures and folding within the fault rupture deformation zone (Figure 3A). The GPR profile runs near the western wall of the trench and shows continuous reflectors which are interpreted as stratigraphic bedding within 5 m of the ground surface. Continuous reflectors marked by dashed white lines in Figure 3B are, for example, correlated with boundaries between sediment packages logged in the trench (Figure 6A). Ground fracturing could also be inferred from the GPR profile, although these inferred fractures were not always observed in the trench walls. The GPR profile was collected prior to trenching and suggested that there may be stratigraphic layers at this site that could provide markers with which to measure displacement (Figure 3A).

Table 1 Summary of OSL samples collected at the trench and quarry sites located in Figure 2.

Site	Location (NZTM)	Laboratory Number‡	Field Number	Depth (m)	Water %	Total Dose Rate (Gy/Ka)	Equivalent Dose (Gy)	Optical Age (ka)†
Highfield	N5172880 E1537010	WLL1048	OSL 1	0.55	10.5	3.59 ± 0.16	77.58 ± 3.65	21.6 ± 1.5
		WLL1049	OSL 3	2.7	19.6	3.30 ± 0.19	108.75 ± 2.62	33.0 ± 2.0
		WLL1050	OSL 4	0.95	21.6	2.66 ± 0.14	85.27 ± 1.97	32.1 ± 1.8
		WLL1051	OSL 6	2.2	9.5	3.70 ± 0.14	104.17 ± 7.74	28.4 ± 2.4
Clintons	N5172701 E1535117	WLL1087	HF 1	1.6	4.7	4.06 ± 0.14	130.98 ± 7.00	32.3 ± 2.1
Quarry	N5172667 E1536137	WLL1097	TCP1	4	14.1	4.17 ± 0.22	89.15 ± 3.90	20.2 ± 1.9
		WLL1098	TCP2	1	10.7	3.62 ± 0.16	84.43 ± 6.59	24.7 ± 1.5

‡ All samples analysed at the Victoria University of Wellington OSL laboratory with measurements taken of blue luminescence from fine-grained feldspar produced during infrared stimulation.

† All ages for Single Aliquot Regeneration method (Wang 2013), reported with 1 sigma uncertainties.

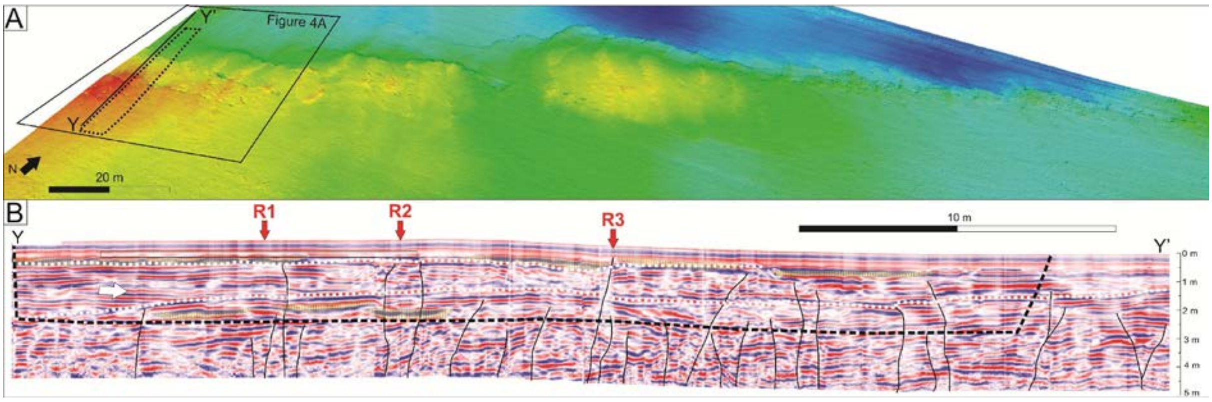

Figure 3 (A) Terrestrial LiDAR image of the farm paddock at Highfield Road that contains the trench site (shown by dashed black rectangle). Image is colour-coded by altitude with red colours approximately 1 m higher in elevation than blue colours. The data were collected within 1 week of the 2010 Darfield earthquake and capture the main features of the surface rupture deformation zone (see also Figure 4 and Figure 6). Profile Y-Y' indicates the location of the GPR profile shown in B. (B) 100 MHz GPR profile that runs along the western wall of the trench. Three major fractures seen at the surface (Riedel shears R1, R2 & R3) and those branching off them were identified, along with many smaller fractures that do not break through the upper ~1.5 m of the gravel (black sub-vertical lines). The main Riedel shears extend to the base of the GPR profile at ~5 m depth. Yellow vertically shaded areas over dark reflectors indicate contrasting sandy layers. Approximate outline of the trench excavated at this site (see Figure 6) is denoted by a dashed black line.

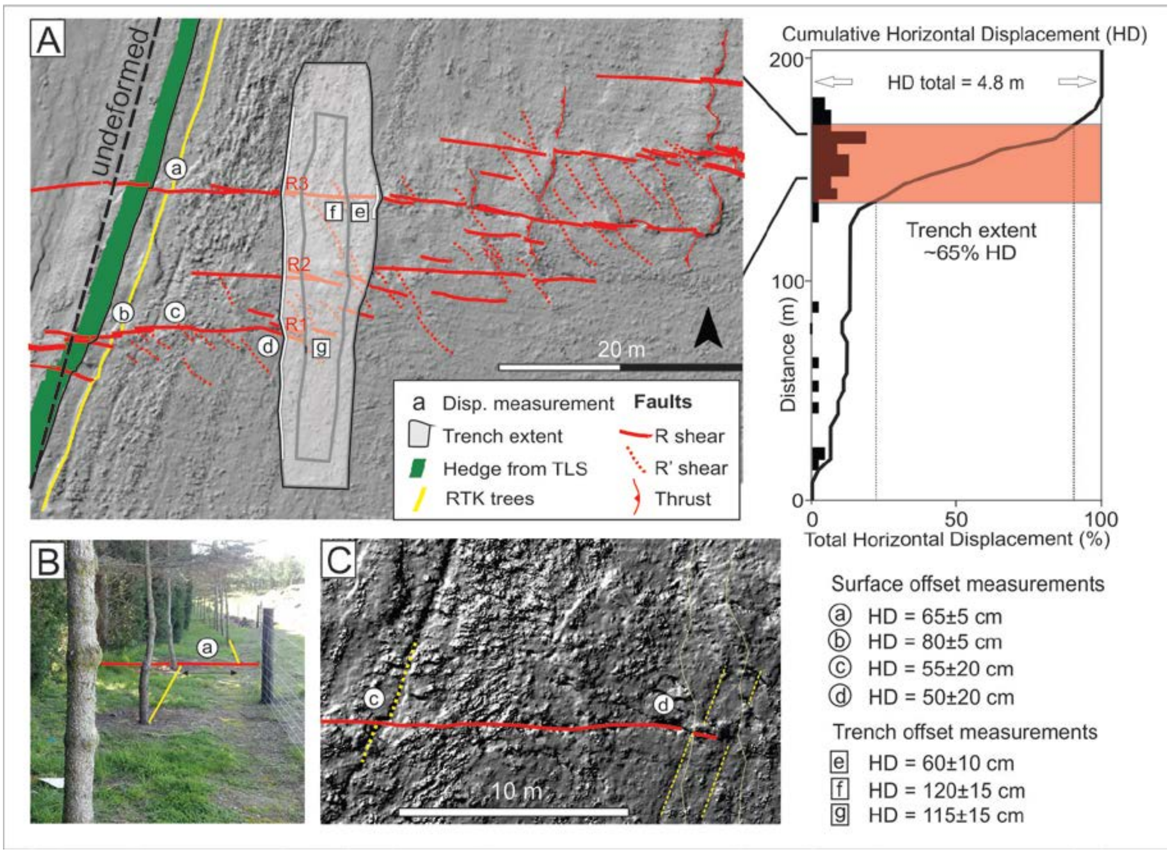

Figure 4 (A) Highfield Road site map showing Riedel shears (red lines) and Riedel prime shears (dashed red lines), displaced cultural markers, and trench location with hill-shaded digital surface model from LiDAR data in the background. Plots are shown of cumulative and incremental (histogram) right-lateral horizontal displacement distribution along the roadside and fence immediately west of the hedge. The trench is located across the highest lateral displacement gradient at the site and its extent is highlighted by the red shading on the cumulative displacement curve. The trench spans ~65% of the total 2010 Darfield earthquake right-lateral displacement at the site (4.8 m), and lateral surface offset on Riedel shears at the site accommodates only about 1/3 of the total lateral displacement. (B) Photograph of tree row (yellow line in A) where it is displaced by the R3 Riedel shear. (C) A plough-line (offset "c") and subtle tyre tracks (offset "d"), visible in close-up of laser scan, are used for estimating offset measurements at the location of the trench.

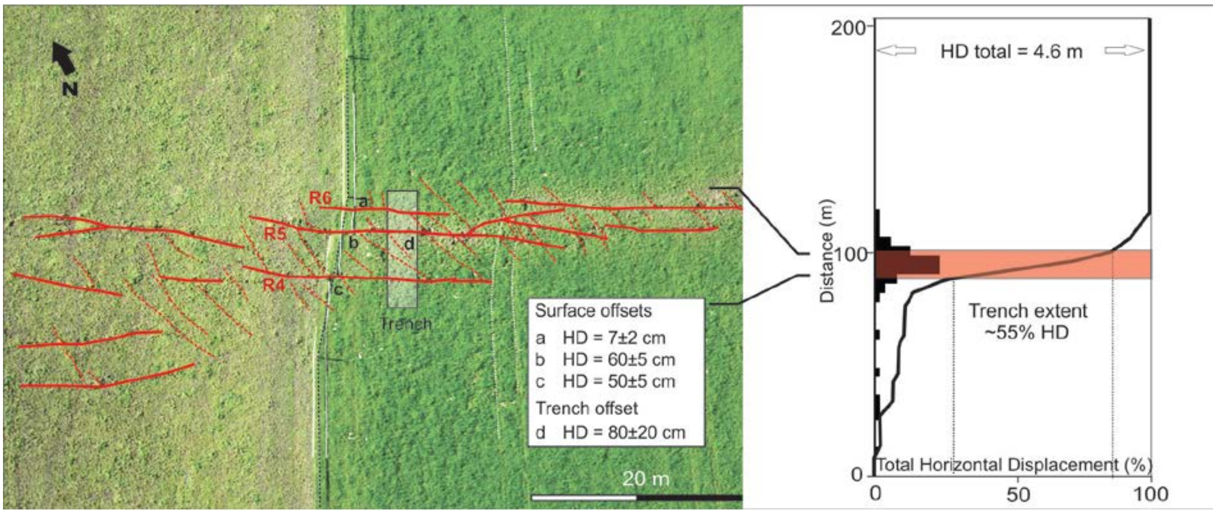

Figure 5 Clintons Road site map of 2010 ground-surface rupture and displaced features on background of post-rupture air-photo. Black dashed line denotes offset fence, and white solid lines on either side denote offset plough-lines. Dashed white lines show tyre tracks deformed right-laterally across the fault trace. Solid red lines are Riedel shears and dashed red lines Riedel prime shears. Plots of cumulative and incremental (histogram) lateral offset show the displacement distribution along the fence line. Right-lateral displacement on discrete structures (Riedel shears) at the site is ~117 cm, which is ~25% of the total 4.6 m strike-slip displacement. The trench is located across the highest displacement gradient at the site, and its extent is highlighted by the red shading on the cumulative displacement curve. The trench spans approximately half (~55%) of the total 2010 Darfield earthquake right-lateral displacement at the site.

At, or immediately adjacent to each trench site, there was excellent characterisation of both the amount and distribution of co-seismic surface rupture displacement generated by the 2010 Darfield earthquake. At both trench sites the total right-lateral displacement is 4.5–5 m and comprises a combination of broad-wavelength folding (i.e., continuous deformation) and discrete faulting (i.e., discontinuous deformation) at length scales of metres to 10s of metres (Figure 4 and Figure 5). The relative contributions of continuous and discontinuous strike-slip deformation are similar at each site: about two-thirds to three-quarters continuous and about one-quarter to one-third discontinuous. The maximum vertical displacement on the fault differs between trench sites being ~0.9 m at Highfield Road and <0.2 m at Clintons Road.

4.1 HIGHFIELD ROAD

This trench is located on a ~500 m long restraining bend along the Greendale Fault (Highfield site, Figure 2). This site was selected for excavation because the majority of the faulting and folding was confined to a relatively narrow zone (<20 m), which contained well defined Riedel shears that could be (hopefully) easily identified in trench walls, while the relatively high vertical component of displacement (~0.9 m) offered the prospect of sediment accumulation on the downthrown side of the fault following paleoearthquakes (Figure 3). In addition, the trench was located close to displaced fences and tree lines that permit accurate measurement of surface rupture displacement in the 2010 Darfield earthquake (Figure 4). Displacements of cultural markers at the ground-surface were used to assess whether displacement of paleo-channels exposed in the trench walls could be accounted for by the 2010 event.

The Highfield Road trench was excavated into gravel-dominated alluvial deposits across the entire width of the zone of ground fracturing (Figure 4 and Figure 6). At a first-order level the stratigraphy comprises stacked cross-bedded fine sand to pebbly gravel beds (20–30 cm thick, with primary stratigraphic dips on cross-bedding ranging between 15 º and 30º) that are locally separated by sub-horizontal gravel beds. These gravel units are overlain by up to

80 cm of silt and silty gravel. Within the gravel-dominated sequence, there are sand-rich lenses of ≥15 cm thickness. Six of these were exposed in the west wall of the trench, four of which are located on the downthrown side of Riedel shear R3 (Figure 6A). The trend of these sand-filled paleo-channels and the imbrication of clasts in the gravel units indicate a general NW to SE paleoflow direction, consistent with the gravels being deposited by the Waimakariri River (Figure 6A). No paleosols were exposed in the trench.

Four lenses of fine to medium grained sand were sampled for OSL dating. Three of these four sampled channels were also measured for their displacements across Riedel shears. These sample locations were chosen because collectively they covered the temporal spread of trench stratigraphy, had similar moisture content (10–20%), and their small particle size made them the most suitable material in the trench for dating. OSL samples 4, 3, and 6 were from approximately similar stratigraphic positions in the trench and yielded ages of 32.1±1.8 ka, 33.0 ± 2.0 ka and 28.4 ± 2.4 ka, respectively (Table 1, see Figure 6A & 6C for locations). The channel marked OSL 1 (Figure 6C) produced an age of 21.6 ± 1.5 ka, consistent with its higher stratigraphic position relative to the samples OSL 4, 3, and 6. Collectively the OSL dates support previously inferred ages for the Burnham Formation (e.g., Forsyth et al., 2008) and suggest alluvial gravel deposition during the LGM. In detail, it is possible that the gravels in the trench were deposited in two episodes at 26–35 ka and post 23 ka, separated by a depositional hiatus or an erosional event.

Tens of faults and fractures were exposed in the walls of the Highfield Road trench (Figure 6A). The most prominent structures in the trench walls were the three Riedel shears observed at the ground surface (R1, R2 and R3; Figure 4 and Figure 6). These shears are spaced at 5–7 m and comprise fault zones up to 0.5 m wide that, at their cores, contain sub-vertical gravel cobbles rotated into parallelism with the fault plane. These shear zones were the only structures that extended from top to bottom of the trench. Two of the three Riedel shears were observed in both walls of the trench (R2 and R3) while the third terminated within the trench (R1; Figure 4 and Figure 6). In addition to the Riedel shears, numerous fractures, often with no discernible vertical displacement in the trench walls, were recorded in the silt, silty gravel and soil A-horizon in the upper 50 to 80 cm of the trench. The localization of small fractures in the upper silty part of the stratigraphic section may have occurred because these materials have a higher unconfined compressive strength (than the underlying loose to slightly compact gravels) and are therefore more likely to deform by brittle failure. Some of the secondary fractures restricted to the upper silty layers were oriented parallel to the R' shears (i.e., the dashed red lines in Figure 5), which strike at a high angle of ~50–70º to the general strike of the fault and at a low angle to the trench walls. Using an intermediate orientation between the R and R′ shears, the maximum compressive stress orientation (σ_1) at the trench site would be ~118º (Figure 6B), which is similar to the regional value of 115 ± 5 º (e.g., Sibson et al., 2011).

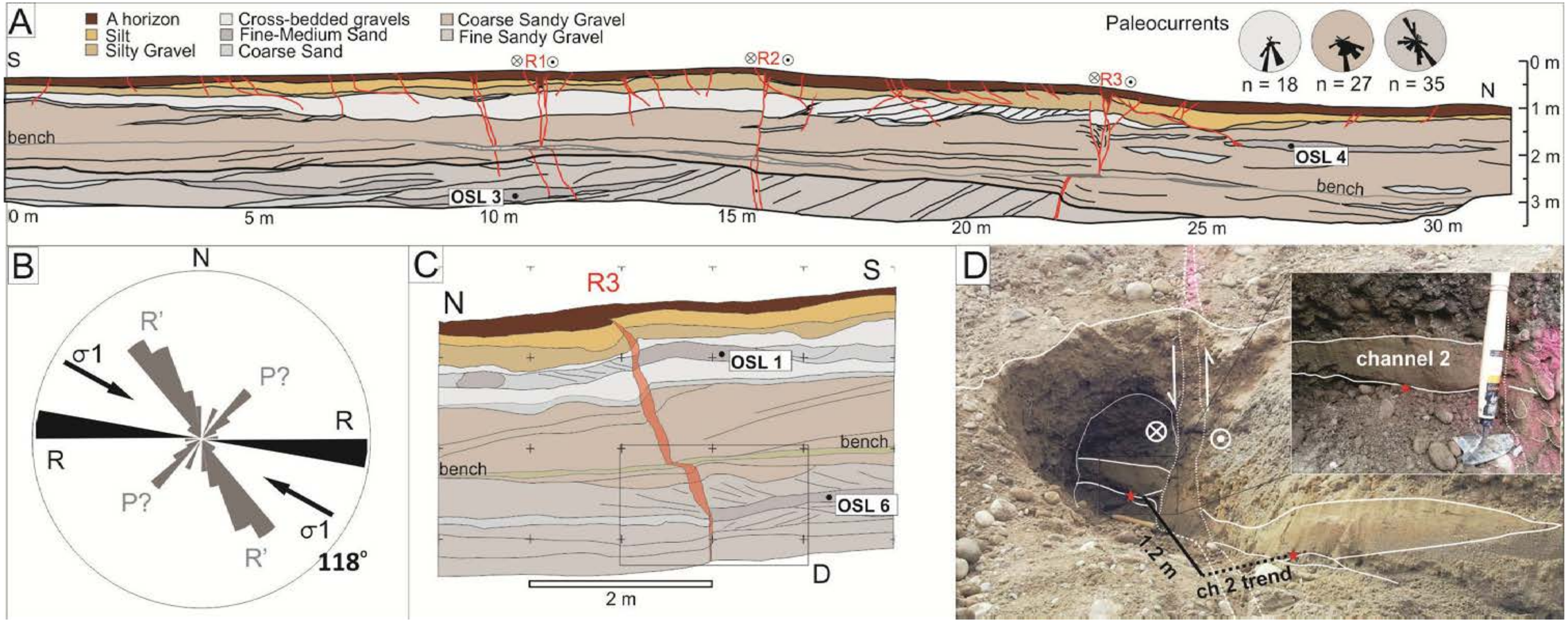

Figure 6 (A) Log of the west wall of the Highfield Road trench. OSL sample locations are marked. Riedel shears (R1, R2 & R3 are labelled) and fractures are shown by the red lines. Paleocurrent directions measured from various units exposed in the trench with colour coding of paleocurrent rose diagram matching colour coding of trench unit lithology. (B) Azimuth of fracture planes recorded in the trench. Riedel (R) shears are shown in black with distribution of Riedel prime (R') and other fracture planes (possibly P shears) in grey. Equidistant between the Riedel and Riedel prime distributions is the inferred σ_1 direction of 118°. (C) Log showing the R3 Riedel shear in the east wall of the trench; key for stratigraphic units is the same for the west wall and locations of OSL are shown. (D) Excavation of the trench wall (location shown in C) to measure offset of sand lens across R3 Riedel shear using piercing point of a gravelly layer at the base of the sand lens. Inset shows appearance of fault at offset edge of sand. Note gravel clasts dragged into sand along the R3 shear, with long axes near-horizontal in slip direction.

Displacements of the ground surface were measured across the entire surface rupture deformation zone and on individual Riedel shears at the Highfield Road site (Figure 4). The total right-lateral displacement across the fault, as measured on the fences and tree lines 15–20 m west of the trench, is 4.8 m. Approximately 1.8 m of right-lateral displacement was accommodated by the Riedel shears which individually accommodate 0.5 to 0.8 m of horizontal displacement and collectively account for about 60% of the total 2.9 m right-lateral displacement encompassed by the trench (see Figure 4 histogram). The remaining strike-slip displacement within the trench was achieved by brittle failure in the upper silty section (<80 cm depth) and throughout the section by folding associated with inelastic inter-granular slip of gravel clasts in an unlithifed/loose sandy matrix. This distributed deformation also accounts for about 70% of the total 0.9 m vertical displacement across the fault zone with the remainder accommodated by approximately 10 cm (down to the north) on each of the three Riedel shears (Figure 4). The available displacement measurements for the entire fault zone and the R3 Riedel shear indicate slip vectors of 075º/11º and 095º/13º, respectively.

In the sub-surface, the R1 and R3 Riedel shears displace a number of sand-filled paleo-channels (Figure 6) that trend at a high angle to the fault (≥~70º), providing piercing points for measuring displacement. Along-strike excavation of the shallower portion of R3 revealed that the eastern margin of the sand lens dated by sample OSL 1 was displaced by 60 cm ± 10 cm (horizontal) and 9 ± 5 cm (vertical). The 60 ± 10 cm right-lateral offset is within error of the 65 ± 20 cm RTK and tape-and-compass measurements of an offset tree line cut by the same (R3) shear 18 m to the west (Figure 4B) and similar to lateral displacements measured on the nearby R1 Riedel shear. Displacements were also measured for two channels deeper in the section than the 'OSL 1' paleo-channel. Both these channels were located within the oldest exposed sedimentary unit in the trench. The channel in the lower east wall (and dated by OSL 6) was displaced by R3 and the channel in the lower west wall (dated by OSL 3) by R1. The axis of the channel displaced by R3 contained a distinctive 18 cm thick silt lens that has been displaced by 120 ± 15 cm horizontally and 21 ± 5 cm vertically. The displacements of this channel are similar to the 115 ± 10 cm horizontal and 20 ± 5 cm vertical displacement on R1 revealed by excavation of the western edge of the sand-filled paleo-channel close to the base of the trench (Figure 6A, OSL 3).

The displacements of the oldest channels on R1 and R3 are approximately double the displacement of the cultural markers at the ground surface and, in the case of R3, the offset of the paleo-channel dated by OSL 1 (Figure 7). The observed up-sequence changes in displacement could be explained by high vertical displacement gradients during a single rupture or by the stratigraphy lower in the trench having experienced multiple earthquake displacements. Given the small vertical separation between the variably displaced beds and the lack of a displacement decrease above the 'OSL 1' lens, we favor the multiple event hypothesis, which is considered further in the "Greendale Fault Penultimate Earthquake and Recurrence Intervals" section.

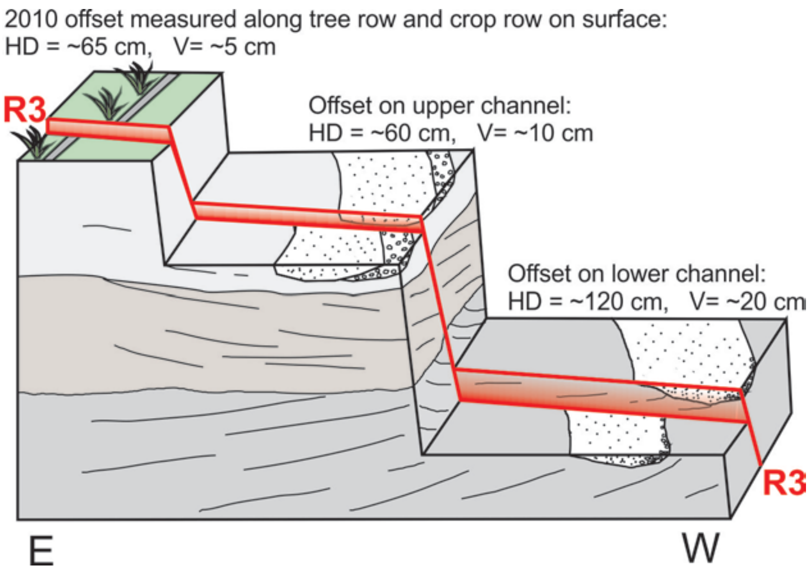

Figure 7 Schematic block diagram showing displaced paleo-channels across R3 Riedel shear at Highfield Road. Layer colours are the same as used in the trench log (Figure 6).

4.2 CLINTONS ROAD

The second trench site, Clintons Road, is located approximately 2 km west of the Highfield Road trench (Figure 2). The site was selected because of its proximity to high-resolution measurements of displaced fence- and plough-lines, the narrow width (<10 m) of the zone of fault fracturing at the ground surface (Figure 5), and the presence of paleo-channels at the ground surface that might have been useful for measuring pre-2010 fault displacements.

The Clintons Road trench exposed gravels similar to those at Highfield Road but, unfortunately, sand lenses that could have been used as displacement markers were not present (Figure 8). The gravel-dominated units at Clintons Road, like those at Highfield Road, comprise alternating cross-bedded units and sub-parallel horizontal units with an absence of paleosols. Imbrication of gravel clasts outside of shear zones indicates paleoflow directions towards the southeast, consistent with the local trend of paleo-channels at the ground surface. One of these channels crosses the northern end of the trench and is filled with silt up to ~20 cm thick (Figure 8A). The gravel units below the silt are subdivided based on changes in primary stratigraphic bed dip, clast size and sand content. In the absence of sand layers, a single OSL sample (HF1) was collected from a gravelly sand approximately 2.5 m below the ground surface (Figure 8D). It yielded an age of 32.3 ± 2.1 ka (Table 1) which is within error of the OSL ages from the lower parts of the Highfield Road trench.

At the Clintons Road trench the fault strikes almost E-W and is expressed as a series of three left-stepping Riedel shears spaced at 3 and 6 m (labeled R4, R5 & R6 in Figure 6). These shears are accompanied by R’ shears that strike at 50º to the Riedel shears. The Riedel shears bound a number of small (~20 m across, ~0.5 m high) push-up structures at restraining stepovers (Figure 2). The R4 and R5 Riedel shears were mapped to the base of the trench at ~ 3 m depth. The expression of the Riedel shears in the subsurface here was very similar to that of the Highfield Road trench, although without any fine-grained units, discrete fault displacements were more challenging to identify and measure. Both the R4 and R5 Riedel shears were observed in the west wall of the trench; however, only R5 could be mapped in the trench’s east wall (Figure 8C). In the trench walls these shears (R4 & R5) were marked by zones up to ~30 cm wide containing clasts that had been rotated from their deposition orientations; in the central ~10 cm of these zones, the clasts have long axes parallel to the sub-vertical shear planes (Figure 8B and Figure 8D). In the upper 1 m of the west wall of the trench, R5 was also characterised by a mixed zone of randomly oriented cobbles and soil which we interpret to be fissure fill. In contrast to the Highfield Road trench, discrete R′ shears were not observed in the trench walls near to the surface, possibly due to the lack of the higher compressive strength silt and silty gravel units below ~30 cm depth in this trench.

Displacements were measured across the entire fault zone and on individual Riedel shears mainly using RTK GPS and tape measurements from a fence-line (and associated plough lines) 4–8 m west of the trench. The total right-lateral displacement across the fault deformation zone is 4.6 m, which was measured over a width of ~120 m perpendicular to fault strike. Approximately 1.8 m of right-lateral displacement was accommodated by the Riedel shears which account for about 25% of the total right-lateral displacement, slightly lower than at Highfield Road where the discrete shears accommodate ~35% of the total right-lateral displacement. Of the total right-lateral displacement, approximately 55% was encompassed by the trench (see Figure 5 histogram). Similar to Highfield Road, the high H:V displacement (20:1) on each Riedel shear meant apparent vertical offsets on cross beds in the trench were a result of the dip of the strata, and actual vertical displacement was very small. Vertical displacement at the site is only 15 cm and approximately 10 cm of this was observed on the discrete Riedel shears.

Discrete lateral displacements on the R4 and R5 Riedel shears at Clintons Road resulting from the 2010 Darfield earthquake are similar to those measured at Highfield Road. The R4 and R5 shears displace the fence and plough lines by 50 ± 5 and 60 ± 5 cm respectively (Figure 5); however, in the absence of terrestrial LiDAR coverage at the site and poorer quality aerial photography than at Highfield Road, no reliable estimates of ground surface offset were possible at the trench site. It was, however, possible to measure sub-surface displacement of one piercing point where it crosses the R5 Riedel shear in the east wall of the trench. The piercing point on R5 was produced by the northern margin of a pea-gravel lens up to 15 cm thick exposed in the trench at 2.5 m depth (Figure 8D and Figure 8E). Careful excavation into the wall of the trench revealed a right-lateral displacement of 80 ± 20 cm for R5 at this location. The low angle of the bed orientation to the fracture coupled with frequent collapse of the granular material made accurate measurement difficult, hence the comparatively large uncertainties. Given the uncertainties in displacement of the pea gravel and the possibility that displacement of the fence (60 ± 5 cm on R5 at the ground surface) may not represent displacement on R5 at the eastern trench wall (the fence is ~7 m west of the trench wall), it remains uncertain whether displacement of the pea gravel occurred in one or more surface-rupturing earthquakes.

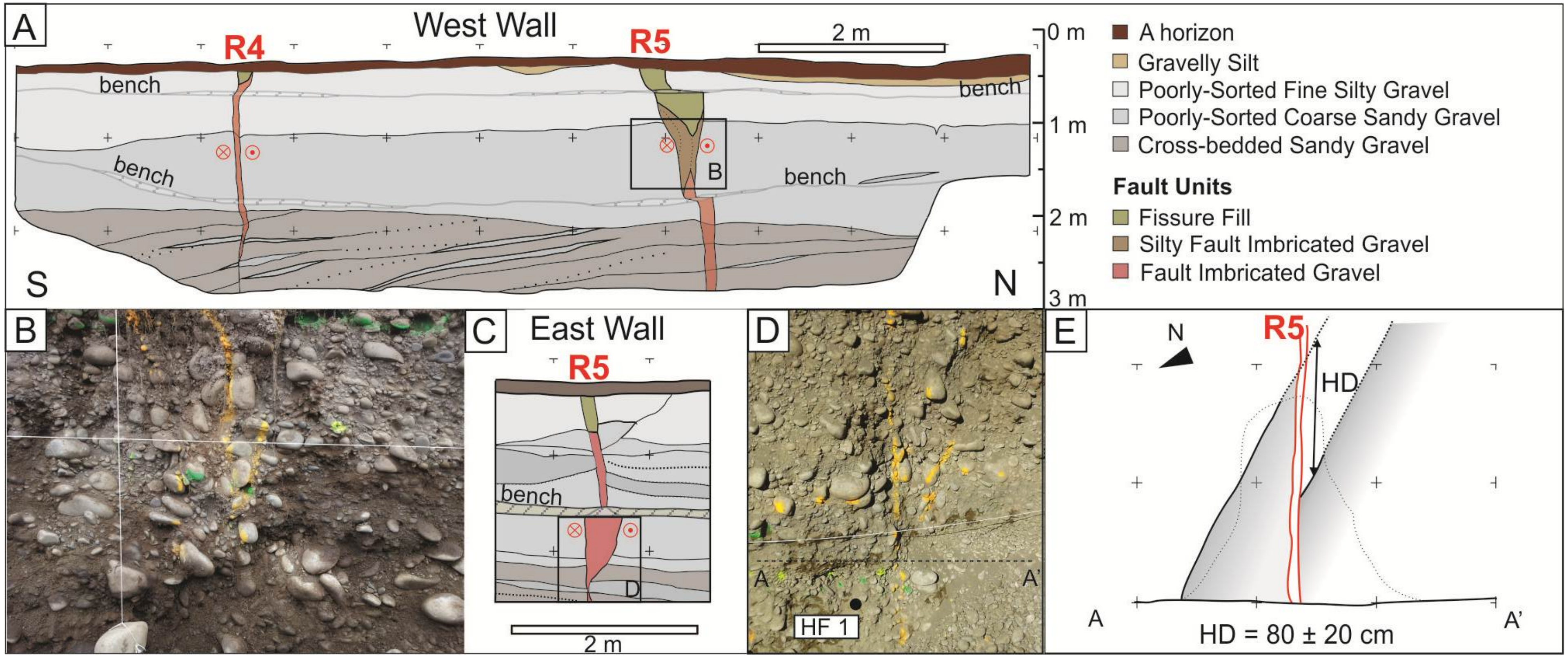

Figure 8 Clintons Road site trench. (A) Log of west wall of trench showing Riedel shears and layered gravel stratigraphy. (B) Fault imbricated gravel clasts showing clast rotation increasing into fault zone (orange spray paint) where their long axes are sub-vertical. (C) Detail of east wall showing multiple sandy gravel layers across the R5 Riedel shear which has variable width. (D) Photo of 'pea gravel' layer in the lower wall (see C for location) that was used for offset measurement, and OSL sample location (HF 1) in gravelly sand immediately below this. (E) Map view of section A-A' showing the 80 ± 20 cm strike-slip displacement of the northern margin of the channel filled with pea gravel in (D). Limits of the excavation shown by the dotted line.

5.0 GREENDALE FAULT PENULTIMATE EVENT, RECURRENCE INTERVAL, AND RECURRENCE INTERVAL CLASS

Following the Darfield earthquake, questions were raised about how many destructive earthquake sources remain undetected close to New Zealand's main cities and how often these sources generate large-magnitude earthquakes. The Canterbury earthquake sequence delineated a number of previously unrecognised active faults, but the slip rates and recurrence intervals on these faults remain largely unresolved. For the Greendale Fault the absence of a clear pre-2010 trace on the Canterbury Plains, mapped locally as Burnham Formation (Villamor et al., 2011), suggests that the penultimate surface-rupturing earthquake predates the final aggradation and abandonment of the Burnham surface at ~16–18 ka (Forsyth et al., 2008), a conclusion that is supported by this study.

At Highfield Road, at least two surface-rupturing earthquakes can be inferred from the doubling of displacements with depth on the R1 and R3 Riedel shears exposed in the trench (Figure 6). While vertical decreases in displacement are commonly inferred for individual earthquakes that rupture the ground surface (e.g., Dolan & Haravitch 2014), and were reported for the Darfield earthquake, these changes typically occur over distances of 100s of metres or kilometres. In the case of the R3 Riedel shear, the 50% reduction in displacement occurs over a vertical distance of ~1.5 m (between sand lenses dated by OSL 1 and OSL 6: Figure 6); however, there is no apparent decrease in displacement between the OSL 1 lens and the ground surface ~60 cm above. The strike-slip displacement gradient for the R3 Riedel shear between the dated sand lenses is 0.4 which is orders of magnitude greater than the gradient of ≤~0.001 estimated from GPS data for a maximum strike-slip of 7 m at a depth of 2 km (Beavan et al., 2010) and 5 m at the ground surface (Quigley et al., 2012). In addition, we can see no evidence of the R1 and R3 Riedel shears bifurcating up-sequence in the trench or transferring displacement to new structures in the upper section of the trench stratigraphy. For these reasons we do not favor using a single event to explain the observed up-sequence decrease in displacement. Currently our preferred interpretation is that older stratigraphy in the Highfield Road trench has experienced a surface-rupturing earthquake in addition to the 2010 event.

If the multiple-event hypothesis is correct, then the ages of the sand lenses dated by the OSL 1 and OSL 6 samples bracket the timing of the penultimate event on the Greendale Fault. These sand lenses have ages of 21.6 ± 1.5 ka (OSL 1) and 28.4 ± 2.4 ka (OSL 6) (Table 1, Figure 9). Taking into account the one sigma uncertainties on the OSL ages, the penultimate event on the Greendale Fault most likely occurred between approximately 20 ka and 30 ka. The location of the event horizon in the trench stratigraphy cannot be determined with confidence. Angular discordance at an erosional contact was noted in the trench <0.8 m above OSL 3 and OSL 6 sand lenses (see thick lines in Figures 6A and 6C), but we cannot demonstrate that it unambiguously represents a significant break in time, or a resolvable increase in the amount of deformation below the contact.

As we only have displacement data for the penultimate event on two Riedel shears at one site where the fault zone is both diffuse and complex, the magnitude of this event remains poorly constrained. Because the postulated earthquake on the Greendale Fault between 20 ka and 30 ka ruptured the ground surface, and historical surface-rupturing earthquakes on reverse and strike-slip faults in New Zealand (i.e., post 1840) were rarely less than M_w 6.5 (Nicol et al., 2012), we suggest that the penultimate event was most likely >M_w 6.5. Given the doubling of displacements on the R1 and R3 Riedel shears in the Highfield Road trench it remains possible that the penultimate surface-rupturing earthquake was similar in displacement and magnitude to the 2010 event (i.e., ~ M_w 7), although more data are required to test this hypothesis.

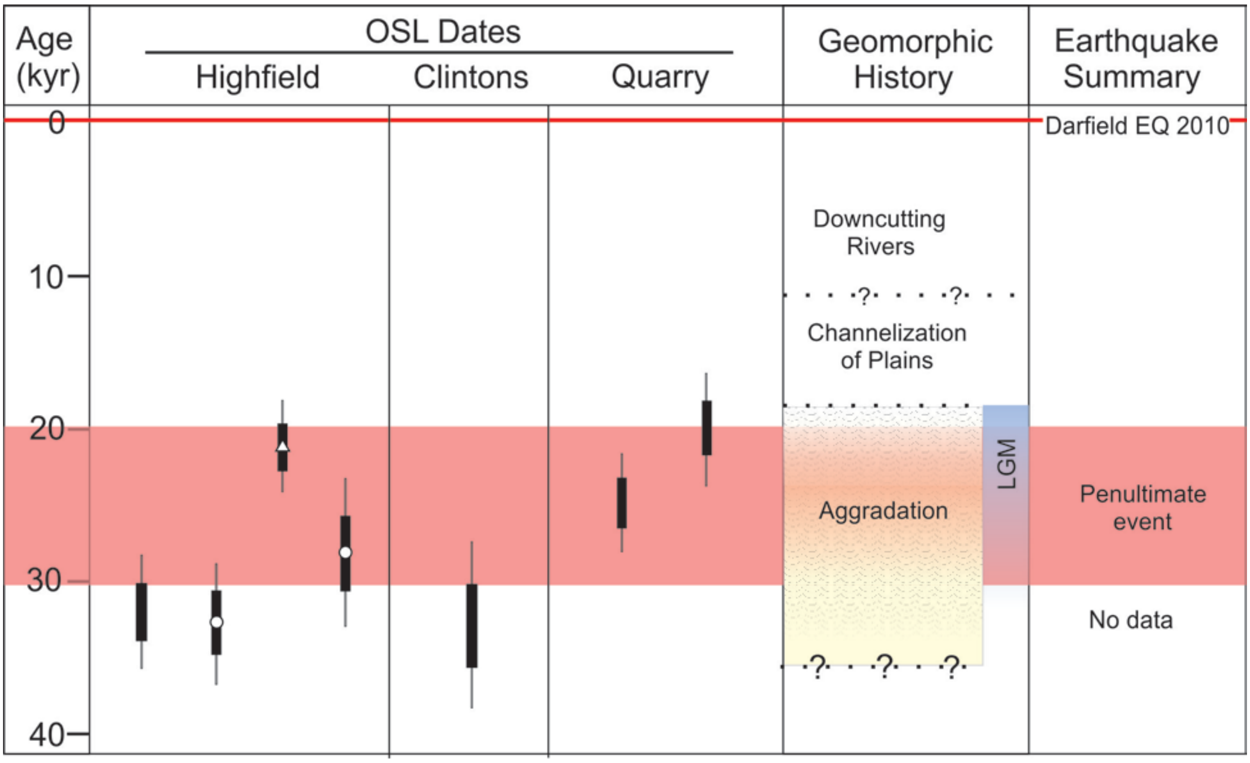

Figure 9 Summary of OSL ages with 1 sigma (black rectangle) and 2 sigma (line) uncertainty bars for stratigraphy at each trench site. White filled circles denote paleo-channels displaced by two or more surface-rupturing earthquakes, and white filled triangle denote paleo-channel displaced by only the 2010 Darfield earthquake. Red polygon shows preferred timing of the penultimate surface-rupture earthquake.

The Greendale Fault has probably ruptured the ground surface repeatedly on prehistoric timescales. A seismic reflection survey across the Greendale Fault along Highfield Road indicates vertical displacement of ~20 to 30 m for inferred Pliocene sediments at depths of ~300 to 400 m (J. Pettinga and D. Lawton, personal communication, 2013). These cumulative subsurface vertical displacements greatly exceed the ~0.4 m average single-event vertical slip at the ground surface in the Darfield earthquake. Assuming sub-horizontal and relatively planar reflector geometries (J. Pettinga, personal communication 2013) and vertical slip gradients comparable to those modelled for the Darfield earthquake (Beavan et al., 2012) it is likely that the Greendale Fault ruptured the ground surface in tens of paleoearthquakes over the last few million years.

If our interpretation that the penultimate surface rupture event on the Greendale Fault occurred between 20 ka and 30 ka is correct, then an indicative range of “permissible” average recurrence intervals for the fault can be estimated by making the following assumptions:

1. Average recurrence interval has a lognormal distribution. Lognormal is a commonly used distribution for average recurrence interval (e.g., Nishenko & Buland 1987; Rhoades et al., 1994, 2011; Van Dissen et al., 2013b), and for our indictive purposes in this report, we consider this an acceptable assumption. For the Greendale Fault this implies that the one inter-event time of 20–30 kyr is part of the lognormal distributions about "permissible" average recurrence intervals.
2. Coefficient of variation (CoV) of average recurrence interval ranges from 0.4 to 0.8. See Dawson et al. (2008) and Nicol et al. (2012) for data and analyses that support this choice of CoV range.
3. The minimum "permissible" average recurrence interval (aveRImin) is within plus one standard deviation of the inter-event time, and the maximum "permissible" average recurrence interval (aveRImax) is within minus one standard deviation of the inter-event time, such that:

   $\ln(\text{aveRImin}) + \sigma = \ln(\text{IET})$, and

   $\ln(\text{aveRImax}) - \sigma = \ln(\text{IET})$

   where σ is the standard deviation, $\sigma = (\ln(\text{CoV}^2 + 1))^{½}$, and IET is inter-event time.

Solving for minimum "permissible" average recurrence interval (aveRImin) and maximum "permissible" average recurrence interval (aveRImax) yields ~10 kyr and ~61 kyr, respectively (Table 2). That is, given the above assumptions, the one Greendale Fault inter-event time of 20–30 kyr is compatible with average recurrence intervals that range between ~10 kyr and ~61 kyr.

Table 2 Greendale Fault average recurrence interval estimation based on a single inter-event time of 20–30 kyr. See text for discussion regarding the assumptions made in order to derive these average recurrence interval values.

Coefficient of Variation (CoV)	minimum average recurrence interval (aveRImin: kyr)			maximum average recurrence interval (aveRImax: kyr)		
	inter-event time (kyr)			inter-event time (kyr)		
	20	25	30	20	25	30
0.4	13.6	17.0	20.4	29.4	36.7	44.1
0.6	11.5	14.4	17.2	34.8	43.5	52.3
0.8	9.9	12.4	14.9	40.9	50.5	60.6

Average recurrence interval, along with fault trace complexity and building importance category, are the three key elements of the New Zealand Ministry for the Environment's active fault guidelines that aim to mitigate the impacts of building on, or near, active faults in New Zealand (Kerr et al., 2004; Van Dissen et al., 2006). In these guidelines, the average recurrence interval of a fault is categorised according to Recurrence Interval Class (RIC), and the guidelines recommend more restrictions on development on, or near, active faults with a low Recurrence Interval Class (e.g., RIC I; faults with average recurrence intervals less than 2000 years), compared to faults with a higher Recurrence Interval Class (e.g., RIC IV; faults with average recurrence intervals between 5000 and 10,000 years). In the aftermath of the Darfield earthquake, and in response to re-build pressures in areas near the Greendale Fault, Environment Canterbury (Canterbury Regional Council) commissioned Villamor et al. (2011) to map the Greendale Fault in accord with the Ministry for the Environment active fault guidelines including delineation of Fault Avoidance Zones along the fault based on fault trace complexity, and definition of Recurrence Interval Class. Villamor et al. (2011) provisionally characterised the Greendale Fault as having a Recurrence Interval Class of RIC IV. They noted, however, that the RIC for the Greendale Fault was poorly constrained, and that additional paleoearthquake data from the fault would be of significant benefit towards a more informed RIC determination. In light of the new information regarding the earthquake rupture history of the Greendale Fault presented in this current report, and with regards to Table 2, we suggest that the Greendale Fault should be re-classified as having a Recurrence Interval Class of RIC V (10,000 to 20,000 years). It is possible that the fault has a recurrence interval greater than 20,000 years, but acknowledging the assumptions made in the recurrence interval derivations presented in Table 2, we consider a conservative classification of RIC V is appropriate.

6.0 DISCUSSION

The five dated OSL samples collected the from the gravel-dominated alluvial sediments exposed in the Highfield and Clintons Road trenches range in age from 21.6 ± 1.5 ka to 32.3 ± 2.1 ka (Table 1), and provide the first numerical age constraints for this portion of the Waimakariari fan, and Burnham Formation. To test the repeatability of these ages, we dated two OSL samples from a nearby gravel quarry (Figure 2). These samples were collected at 1 m and 4 m depth from sand lenses within gravel-dominated deposits identical to those exposed in the Highfield and Clintons Road trenches, and retuned ages of 24.7 ± 1.5 ka, and 20.2 ± 1.9 ka respectively (Table 1). Collectively the OSL ages listed in Table 1 confirm that this portion of the Waimakariari fan was actively aggrading over the time period of ~20–32 ka; they also confirm the LGM age previously assigned for the Burnham Formation (e.g., Alloway et al., 2007; Forsyth et al., 2008) (Figure 9).

The long elapsed time between the last two surface-rupturing events on the Greendale Fault, the assumed low slip rates and the predominance of strike-slip likely promote the poor preservation of the fault at the ground surface. An additional factor contributing to the concealment of the fault was the relative timing of the penultimate surface rupture and alluvial fan aggradation by the Waimakariri River on the Canterbury Plains. Based on OSL dates of the gravel-dominated units exposed in the trenches and the analysis of displacements on the Riedel shears in the Highfield Road trench, the penultimate surface-rupturing earthquake on the Greendale Fault occurred during a period when the alluvial fans were actively building the surface of the Plains (Figure 9). Under these high energy conditions a fault scarp of 1 m or less in height could be expected to be buried or eroded rapidly. The relative importance of burial and erosion may have varied along the fault trace depending on a number of factors including the scarp height, relief on the fan surface immediately prior to the fault rupture and fluctuations in river bed-load through time. Inspection of the two trenches excavated across the Greendale Fault provide no clear evidence that the fault scarp for the penultimate event survived its encounter with the ancestral Waimakariri River; however, the scarp height was likely small (<1 m) and identifying a scarp in gravel dominated stratigraphy is not straight-forward. Despite these problems in recognizing a pre-existing fault scarp, the general absence of paleosols within the sedimentary units exposed in the trenches seems to require some erosion and scarp modification during alluvial fan building over a time interval of up to 15 kyr (Figure 9).

Displacement on the central Greendale Fault is dominated by broad wavelength folding (termed "horizontal flexure" in Van Dissen et al., 2013a) (see Figures 4 and 5). By trenching a historic rupture with highly accurate surface displacement data from LiDAR, RTK GPS, and field tape and compass measurements, we provide detailed analysis of the breakdown of total offset into different forms of displacement. Displacement on Riedel shears at the two trench sites made up only a quarter to a third of total displacement, despite the fact that both trenches were selected because shear strains were focused into relatively narrow zones. These observations have two possible implications for paleoseismic studies of active faults that cut through thick (>100 m) unconsolidated Quaternary sediments. First, in these sedimentological settings trenches 10–20 m in length may only sample part of the fault zone and could miss key components of the deformation field. Second, exceptional preservation of geomorphic displacement markers will be required in the geological record to accurately describe the width of the fault zone and the distribution of displacement within this zone. Potential difficulties in recognizing and accurately mapping displacements across such active fault zones could lead to underestimates of the total and average displacement on the fault.

Dolan & Haravitch (2014) discuss the difference between offset on discrete structures versus distributed deformation with implications for underestimation for paleoearthquake displacement and magnitude. The wealth of accurate offset data from LiDAR and ground based RTK measurement of almost totally straight anthropogenic markers (power pole arrays, paddock fences, roads), directly compared with trenching of the fault, allow for unprecedented data collection and new insight into this problem. The data show a clear dichotomy between what we know about the magnitude of historic surface rupture and what we are able to discern of the modern surface rupture in a carefully excavated and located trench.

The 2010 Darfield M_w 7.1 earthquake is an example of a growing list of events worldwide that rupture faults that were not previously known to exist. In New Zealand, for example, in the post 1840 AD time interval, only ~60% of shallow (< 30 km) historical earthquakes of magnitude 7 or greater occurred on faults that have been sufficiently well mapped using modern techniques to show that they are capable of generating large-magnitude events. Given these sampling issues, both the size of the hazard represented by these unsampled faults and the ability of background seismicity models to account for these hazards remain uncertain. Reducing these uncertainties will be a focus of future seismic hazard research.

Accurately determining the seismic hazards for Christchurch city requires an improved understanding of the number and locations of these possible large earthquake sources (i.e., active faults). Given the large size of the Plains (7500 km^2) (Browne & Naish 2012) and the current expense of collecting sub-surface information (e.g., seismic reflection profiles), it seems unlikely that it will be possible to identify and map all of the concealed structures in the next 10–20 years. Comparison of regional GPS strain data and displacement during the Darfield earthquake provides a means of estimating the possible number of Darfield-sized earthquakes over the last 16–18 ka (i.e., the timing of abandonment of the Canterbury Plains alluvial fan surfaces). Wallace et al. (2007) indicate a rate of convergence across the Canterbury Plains block, east of Porters Pass to Amberley Fault Zone (see Figure 1 for location), of about 2 mm/yr trending at 115 ± 5º. Beavan et al. (2012) document ~3000 mm of ESE shortening across the Greendale Fault during the Darfield event (between the GPS survey points shown in Figure 1), which at 2 mm/yr represents 1500 years of accumulated strain. Assuming that the rates of GPS shortening apply to the long-term and that these strains will mainly be converted to permanent strain during large-magnitude earthquakes (neither of which has been tested), would suggest up to 12 Darfield size earthquakes every 18 kyr. Geological mapping prior to 2010 revealed few active faults on the Canterbury Plains from which it might be concluded that much of the 2 mm/yr identified in the GPS signal is accommodated in the foothills along the western margin of the Plains and/or on structures beneath the Plains that do not rupture the ground surface and have sufficiently low slip rates that they do not produce topographic relief. For example, two moderate historical earthquakes (M_w 4.7–4.9 Christchurch; M_w 5.6–5.8 Lake Ellesmere) occurred in the Plains area on unknown (presumably blind) faults in 1869 and 1870 (Downes & Yetton 2012) and similar events could accommodate some of the strain budget identified by the GPS surveys. However the shortening accrues across the Canterbury Plains region through time, and on which structures, it is clear that significant gaps still exist in our understanding of active faulting in this region.

7.0 CONCLUSIONS

1. The previously unknown Greendale Fault ruptured the ground surface in the September 2010 moment magnitude (M_w) 7.1 Darfield Earthquake, producing a fault zone up to 300 m wide that comprised both discrete (faulting) and distributed (folding) deformation dominated by right-lateral displacement.
2. Discrete surface fracturing, when present, accommodates an average of ~30% of the total right-lateral displacement with the remainder taken up by broad wavelength folding about vertical hinges accompanied by slip between gravel clasts.
3. Comparison of Riedal shear displacement of buried paleo-channels with displacement of agricultural markers (e.g., fences, roads and plough lines) suggests multiple surface rupturing earthquakes on the Greendale Fault.
4. Optically stimulated luminescence (OSL) dating of paleo-channels with factor-of-two differences in strike-slip and vertical displacements suggests that the penultimate surface rupturing event on the fault probably occurred between ~20 and 30 ka.
5. The one Greendale Fault inter-event time of 20–30 kyr is compatible with calculated average recurrence intervals that range between ~10 kyr and ~61 kyr, assuming that average recurrence interval has a lognormal distribution, the coefficient of variation of average recurrence interval ranges from 0.4 to 0.8, the minimum “permissible” average recurrence interval is within plus one standard deviation of the inter-event time, and the maximum “permissible” average recurrence interval is within minus one standard deviation of the inter-event time.
6. We suggest that the Greendale Fault should be re-classified as having a Recurrence Interval Class of RIC V (10,000 to 20,000 years), compared to the previous provisional estimation of RIC IV (5000 to 10,000 years).
7. The Greendale Fault remained undetected prior to the Darfield earthquake because the penultimate fault scarp was eroded and buried during Late Pleistocene alluvial aggradation. Similar active faults with low slip rates (i.e., lower than the rates of sedimentation or erosion) are likely to be concealed in alluvial settings globally.

8.0 ACKNOWLEDGEMENTS

This research was funded by The Earthquake Commission (EQC) of New Zealand and by a GNS Science Sarah Beanland Scholarship (SH). We are grateful to Robert Langridge and Dougal Townsend for their reviews of the manuscript.

9.0 REFERENCES

Alloway, B.V., D.J. Lowe, D.J.A. Barrell, R.M. Newnham, P.C. Almond, P.C. Augustinus, N.A.N. Bertler, L. Carter, N.J. Litchfield, M.S. McGlone, J. Shulmeister, M.J. Vandergoes, P.W. Williams, B. Anderson, H. Brackley, P. Burge, J. Carter, U. Cochran, P. Cooke, J. Crampton, E. Crouch, M. Crundwell, Y. Deng, F. Drost, I. Graham, M. Harper, B. Hayward, C. Hendy, C. Hollis, M. Hughes, D. Kennedy, L. Kennedy, D. King, A. Mackintosh, B. Manighetti, M. Marra, D. Mildenhall, U. Morgenstern, T. Naish, H. Neil, D. Nobes, M. Page, A. Palmer, C. Prior, U. Rieser, H. Rother, P. Shane, P. Strong, P. Suggate, J. Thomson, P. Tonkin, N. Trustrum, R. Van Dissen, C. Vucetich, J. Wilmshurst, C. Woodward, and A. Zondervan (2007). Towards a climate event stratigraphy for New Zealand over the past 30 000 years (NZ-INTIMATE project), *J. Quaternary Sci.* **22,** no. 1, 9-35.

Balfour, N.J., M.K. Savage, and J. Townend (2005). Stress and crustal anisotropy in Marlborough, New Zealand: Evidence for low fault strength and structure-controlled anisotropy, *Geophys. J. Int.* **163,** 1073-1086.

Bannister, S., and K. Gledhill (2012). Evolution of the 2010–2012 Canterbury earthquake sequence, *New Zeal. J. Geol. Geophys.* **55,** no. 3, 295-304.

Barrell, D.J.A., Litchfield, N.J., Townsend, D.B., Quigley, M., Van Dissen, R.J., Cosgrove, R., Cox, S.C., Furlong, K., Villamor, P., Begg, J.G., Hemmings-Sykes, S., Jongens, R., Mackenzie, H., Noble, D., Stahl, T., Bilderback, E., Duffy, B., Henham, H., Klahn, A., Lang, E.M.W., Moody, L., Nicol, R., Pedley, K., Smith, A. (2011). Strike-slip ground-surface rupture (Greendale Fault) associated with the 4 September 2010 Darfield earthquake, Canterbury, New Zealand, *Q. J. Eng. Geol. Hydroge.* **44**, 283-291.

Beavan, J., P.Tregoning, M. Bevis, T. Kato, and C. Meertens (2002). Motion and rigidity of the Pacific Plate and implications for plate boundary deformation, *Geophys. Res. B Solid Earth* **107,** no. B10, ETG-19.

Beavan, J., L. Wallace, S. Samsonov, S. Ellis, M. Motagh, and N. Palmer (2010). The Darfield (Canterbury) earthquake: geodetic observations and preliminary source model, *Bull. New Zeal. Soc. Earthq. Eng.* **4,** no. 4, 228.

Beavan, J., M. Motagh, E.J. Fielding, N. Donnelly, and D. Collett (2012). Fault slip models of the 2010–2011 Canterbury, New Zealand, earthquakes from geodetic data and observations of postseismic ground deformation, *New Zeal. J. Geol. Geophys.* **55,** no. 3, 207-221

Bradley, B.A., M.C. Quigley, R.J. Van Dissen, and N.J. Litchfield (2014). Ground motion and seismic source aspects of the Canterbury earthquake sequence, *Earthq. Spectra* **30**, no. 1, 1-15.

Bray, J.D., and K.I. Kelson (2006). Observations of surface fault rupture from the 1906 earthquake in the context of current practice, *Earthq. Spectra* **22,** no. S2, 69-89.

Brown, L.J., and J.H. Weeber (1992). *Geology of the Christchurch urban area,* M. B. Reay (Ed.), Institute of Geological and Nuclear Sciences.

Browne, G.H., and T.R. Naish (2003). Facies development and sequence architecture of a late Quaternary fluvial-marine transition, Canterbury Plains and shelf, New Zealand: implications for forced regressive deposits, *Sediment. Geol.* **158,** no. 1-2, 57-86.

Browne, G.H., B.D. Field, D.J.A. Barrell, R. Jongens, K.N. Bassett, and R.A. Wood (2012). The geological setting of the Darfield and Christchurch earthquakes, *New Zeal. J. Geol. Geophys.* **55,** no. 3, 193–197.

Calais, E., A. Freed, G. Mattioli, F. Amelung, S. Jónsson, P. Jansma, S.H. Hong, T. Dixon, C. Prépetit, and R. Momplaisir (2010). Transpressional rupture of an unmapped fault during the 2010 Haiti earthquake. *Nat. Geosci.* **3**, 794-799.

Campbell, J., J. Pettinga, and R. Jongens (2012). The tectonic and structural setting of the 4th September 2010 Darfield (Canterbury) Earthquake sequence, New Zealand. *New Zeal. J. Geol. Geophys.* **55,** no. 3, 155–168.

Cox, S., and D.J.A. Barrel (2007). Geology of the Aoraki area, Institute of Geological and Nuclear Sciences 1: 250000 Geological Map. *Lower Hutt, New Zealand.*

Dawson, T.E., R.J. Weldon, and G.P. Biasi (2008). Recurrence interval and event age data for Type A faults, Appendix B in The Uniform California Earthquake Rupture Forcast, version 2 (UCERF 2): U.S. Geological Survey Open-File Report 2007-1437B and California Geological Survey Special Report 203B, 48 p. [http://pubs.usgs.gov/of/2007/143/b/].

Davy, B., V. Stagpoole, D. Barker, and J. Yu (2012). Subsurface structure of the Canterbury region interpreted from gravity and aeromagnetic data, *New Zeal. J.Geol. Geophys.* **55**, no. 3, 185-191.

DeMets, C., R.G. Gordon, and D.F. Argus (2010). Geologically current plate motions, *Geophys. J. Int.***181,** 1-80.

Dolan, J.F., and B.D. Haravitch (2014). How well do surface slip measurements track slip at depth in large strike-slip earthquakes? The importance of fault structural maturity in controlling on-fault slip versus off-fault surface deformation, *Earth Planet. Sc. Lett.* **388**, 38-47.

Dorn, C., A.G. Green, R. Jongens, S. Carpentier, A.E. Kaiser, F. Campbell, M. Finnemore, and J. Pettinga (2010). High-resolution seismic images of potentially seismogenic structures beneath the northwest Canterbury Plains, New Zealand, *J. Geophys. Res. B Solid Earth*, **115,** no. B11.

Downes, G., and M. Yetton (2012). Pre-2010 historical seismicity near Christchurch, New Zealand: the 1869 M_w 4.7–4.9 Christchurch and 1870 M_w 5.6–5.8 Lake Ellesmere earthquakes, *New Zeal. J. Geol. Geophys.* **55,** no. 3, 199-205.

Duffy, B., M. Quigley, D. Barrell, R. Van Dissen, T. Stahl, S. Leprince, C. McInnes, and E. Bilderback (2013). Fault kinematics and surface deformation across a releasing bend during the 2010 M_w 7.1 Darfield, New Zealand, earthquake revealed by differential LiDAR and cadastral surveying, *GSA. Bulletin* **125**, 420-431.

Eberhart-Phillips, D., and S. Bannister (2002). Three-dimensional crustal structure in the Southern Alps region of New Zealand from inversion of local earthquake and active source data, *J. Geophys. Res.* **107**.

Elliott, J.R., E.K. Nissen, P.C. England, J.A. Jackson, S. Lamb, Z. Li, M. Oehlers, and B. Parsons (2012). Slip in the 2010–2011 Canterbury earthquakes, New Zealand, *J. Geophys. Res. B Solid Earth* **117**, no. B3

Field, B.D., G.H. Browne, B. Davy, R.H. Herzer, R.H. Hoskins, J.L. Raine, G.J. Wilson, R. J. Sewell, D. Smale, and W.A. Watters (1989). Cretaceous and Cenozoic sedimentary basins and geological evolution of the Canterbury region, South Island, New Zealand, *New Zealand Geological Survey Basin Studies 2*. Wellington, New Zealand: Department of Scientific and Industrial Research, 94 pp.+ enclosures.

Fielding, E.J., P.R. Lundgren, R. Bürgmann, and G.J. Funning (2009). Shallow fault-zone dilatancy recovery after the 2003 Bam earthquake in Iran, *Nature* **458**, no. 7234, 64-68.

Forsyth, P.J., D.J.A. Barrell, and R. Jongens (2008). Geology of the Christchurch area, Institute of Geological and Nuclear Sciences 1: 250000 Geological Map. *Lower Hutt, New Zealand.*

Fry, B., and M.C. Gerstenberger (2011). Large apparent stresses from the Canterbury earthquakes of 2010 and 2011, *Seismol. Res. Lett.* ***82,*** no. 6, 833-838.

Ghisetti, F., and R. Sibson (2012). Compressional reactivation of E–W inherited normal faults in the area of the 2010–2011 Canterbury earthquake sequence, *New Zeal. J. Geol. Geophys.* **55,** no. 3, 177-184.

Holden, C., J. Beavan, B. Fry, M. Reyners, J. Ristau, R. Van Dissen, P. Villamor, and M. Quigley (2011). Preliminary source model of the M_w 7.1 Darfield earthquake from geological, geodetic and seismic data. in *Ninth Pacific Conference on Earthquake Engineering, Building an Earthquake-Resilient Society,* Auckland, New Zealand, Paper 164, 8 p.

Jongens, R., J. Pettinga, and J. Campbell (1999). Stratigraphic and structural overview of the onshore Canterbury Basin: North Canterbury to the Rangitata River. Report prepared for Indo-Pacific Energy Ltd., (Permit PEP38256), p.31.

Jongens, R., D.J.A. Barrell, J.K. Campbell, and J.R. Pettinga (2012). Faulting and folding beneath the Canterbury Plains identified prior to the 2010 emergence of the Greendale Fault, *New Zeal. J. Geol. Geophys.* **55**, no. 3, 169-176.

Kaiser, A., C. Holden, J. Beavan, D. Beetham, R. Benites, A. Celentano, D. Collet, J. Cousins, M. Cubrinovski, G. Dellow, P. Denys, E. Fielding, B. Fry, M. Gerstenberger, R. Langridge, C. Massey, M. Motagh, N. Pondard, G. McVerry, J. Ristau, M. Stirling, J. Thomas, SR. Uma, and J. Zhao (2012). The M_w 6.2 Christchurch earthquake of February 2011: preliminary report, *New Zeal. J. Geol. Geophys.* **55**, no. 1, 67-90.

Kerr, J., S. Nathan, R. Van Dissen, P. Webb, D. Brunsdon, and A King (2004). Planning for development of land on or close to active faults: A guideline to assist resource management planners in New Zealand, Published by the Ministry for the Environment ME number 565, 67 p.

Litchfield, N.J., R.J. Van Dissen, S. Hornblow, M. Quigley, and G. Archibald (2014a). Detailed analysis of Greendale Fault ground surface rupture displacement and geometries, *GNS Science Report* 2013/18

Litchfield, N.J., R. Van Dissen, R. Sutherland, P.M. Barnes, S.C. Cox, R. Norris, J. Beavan, R. Langridge, P. Villamor, K. Berryman, M. Stirling, A. Nicol, S. Nodder, G. Lamarche, D.J.A. Barrell, J.R. Pettinga, T. Little, N. Pondard, J.J. Mountjoy, and K. Clark (2014b). A model of active faulting in New Zealand, *New Zeal. J. Geol. Geophys.* **57**, no. 1, 32-56.

Liu-Zeng, J., L. Wen, J. Sun, Z. Zhang, G. Hu, X. Xing, L. Zeng, and Q. Xu (2010). Surficial slip and rupture geometry on the Beichuan fault near Hongkou during the M_w 7.9 Wenchuan earthquake, China, *Bull. Seismol. Soc. Am.* **100**, no. 5B, 2615-2650.

McCalpin, J.P., T.K. Rockwell, and R.J. Weldon (1996). Paleoseismology of strike-slip tectonic environments, Chapter 6, in *Paleoseismology,* J. P. McCalpin (Editor), Academic Press, San Diego, California, 271-329.

Nishenko, S.P., and R. Buland, R. (1987). A generic recurrence interval distribution for earthquake forecasting, *Bull. Seismol. Soc. Am.* **77**, 1382-1399.

Nicol, A., (1993). Haumurian (c.66-80 Ma) half-graben development and deformation, mid Waipara, north Canterbury, New Zealand, *New Zeal. J. Geol. Geophys*. **36,**127–130.

Nicol, A., and D.U. Wise (1992). Paleostress adjacent to the Alpine Fault of New Zealand: fault, vein, and styolite data from the Doctors Dome Area, *J. Geophys. Res. B Solid Earth* **97**, no. B12, 17685-17692.

Nicol, A., R. Robinson, R. Van Dissen, and A. Harvison (2012). Variability in slip/event and recurrence intervals for large magnitude paleoearthquakes on New Zealand's active faults, *GNS Science Report* 2012/41, 57p.

Norris, R. J., and A.F. Cooper (2001). Late Quaternary slip rates and slip partitioning on the Alpine Fault, New Zealand, *J. Struct. Geol.* **23,** 507-520.

Oskin, M.E., J.R. Arrowsmith, A.H. Corona, A.J. Elliott, J.M. Fletcher, E.J. Fielding, P.O. Gold, J.J.G. Garcia, K.W. Hudnut, J. Liu-Zeng, and O.J. Teran (2012). Near-field deformation from the El Mayor–Cucapah earthquake revealed by differential LIDAR, *Science* **335**, no. 6069, 702-705.

Pettinga, J.R., M.D. Yetton, R.J. Van Dissen, and G. Downes (2001). Earthquake source identification and characterisation for the Canterbury region, South Island, New Zealand, *Bull. New Zeal. Soc. Earthq. Eng.* **34,** 282-317.

Quigley, M., R. Van Dissen, P. Villamor, N. Litchfield, D. Barrell, K. Furlong, T. Stahl, B. Duffy, E. Bilderback, D. Noble, D. Townsend, J. Begg, R. Jongens, W. Ries, J. Claridge, A. Klahn, H. Mackenzie, A. Smith, S. Hornblow, R. Nicol, S. Cox, R. Langridge, and K. Pedley (2010a). Surface rupture of the Greendale Fault during the M_w 7.1 Darfield (Canterbury) Earthquake, New Zealand: initial findings, *Bull. New Zeal. Soc. Earthq. Eng.* **43**, 236-242.

Quigley, M., P. Villamor, K. Furlong, J. Beavan, R. Van Dissen, N. Litchfield, T. Stahl, B. Duffy, E. Bilderback, D. Noble, D. Barrell, R. Jongens, and S. Cox (2010b). Previously unknown fault shakes New Zealand's South Island, *Eos Trans. AGU.* **91**, no. 49, 469-470.

Quigley, M., R. Van Dissen, N. Litchfield, P. Villamor, B. Duffy, D. Barrell, K. Furlong, T. Stahl, E. Bilderback, and D. Noble (2012). Surface rupture during the 2010 M_w 7.1 Darfield (Canterbury) earthquake: Implications for fault rupture dynamics and seismic-hazard analysis, *Geology* **40,** 55-58.

Reyners, M., D. Eberhart-Phillips, and S. Martin (2014). Prolonged Canterbury earthquake sequence linked to widespread weakening of strong crust, *Nat. Geosci.* **7,** no. 1, 34-37.

Rhoades, D.A., R.J. Van Dissen, and D.J. Dowrick (1994). On the handling of uncertainties in estimating the hazard of rupture on a fault segment, *J. Geophys. Res.* **99** (B7), 13,701-13,712.

Rhoades, D.A., R.J. Van Dissen, R.M. Langridge, T.A. Little, D. Ninis, E.G.C. Smith, and R. Robinson (2011). Re-evaluation of conditional probability of rupture of the Wellington-Hutt Valley segment of the Wellington Fault, *Bull. New Zeal. Soc. Earthq. Eng.* **44**, 77-86.

Rockwell, T.K., S. Lindvall, T. Dawson, R. Langridge, W. Lettis, and Y. Klinger (2002). Lateral offsets on surveyed cultural features resulting from the 1999 Izmit and Düzce earthquakes, Turkey, *Bull. Seismol. Soc. Am.* **92**, 79-94.

Rockwell, T.K., and Y. Klinger (2013). Surface rupture and slip distribution of the 1940 Imperial Valley earthquake, Imperial Fault, Southern California: Implications for rupture segmentation and dynamics, *Bull. Seismol. Soc. Am.* **103**, 629-640.

Sibson, R., F. Ghisetti, and J. Ristau (2011). Stress control of an evolving strike-slip fault system during the 2010–2011 Canterbury, New Zealand, earthquake sequence, *Seismol. Res. Lett.* **82,** no. 6, 824-832.

Sibson, R.H., F.C. Ghisetti, and R.A. Crookbain (2012). Andersonian wrench faulting in a regional stress field during the 2010–2011 Canterbury, New Zealand, earthquake sequence, *Spec. Publ. Geol. Soc. Lond.* **367**, no. 1, 7-18.

Stirling, M., and M. Gerstenberger (2010). Ground motion–based testing of seismic hazard models in New Zealand, *Bull. Seis. Soc. Am.***100,** 1407-1414.

Stirling, M., G. McVerry, M. Gerstenberger, N. Litchfield, R. Van Dissen, K. Berryman, P. Barnes, L. Wallace, P. Villamor, R. Langridge, G. Lamarche, S. Nodder, M. Reyners, B. Bradley, D. Rhoades, W. Smith, A. Nicol, J. Pettinga, K. Clark, and K. Jacobs (2012). National seismic hazard model for New Zealand: 2010 update, *Bull. Seis. Soc. Am.* **102**, 1514-1542.

Syracuse, E.M., C.H. Thurber, C.J. Rawles, M.K. Savage, and S. Bannister (2013). High- resolution relocation of aftershocks of the Mw 7.1 Darfield, New Zealand, earthquake and implications for fault activity, *J. Geophys. Res. Solid. Earth*, **118,** no. 8, 4184-4195.

Townend, J., S. Sherburn, R. Arnold, C. Boese, and L. Woods (2012). Three-dimensional variations in present-day tectonic stress along the Australia–Pacific plate boundary in New Zealand, *Earth Planet. Sc. Lett.* **353,** 47-59.

Van Dissen, R., D. Heron, J. Becker, A. King, and J. Kerr (2006). Mitigating active fault surface rupture hazard in New Zealand: development of national guidelines, and assessment of their implementation. in proceedings, 8th U.S. National Conference on Earthquake Engineering, San Francisco, California, 18-22 April, 2006. Paper No. 633, 10 p.

Van Dissen, R., D. Barrell, N. Litchfield, P. Villamor, M. Quigley, A. King, K. Furlong, J. Begg, D. Townsend, H. Mackenzie, T. Stahl, D. Noble, B. Duffy, E. Bilderback, J. Claridge, A. Klahn, R. Jongens, S. Cox, R. Langridge, W. Ries, R. Dhakal, A. Smith, S. Hornblow, A. Nicol, and K. Pedley (2011). Surface rupture displacement on the Greendale Fault during the Mw 7.1 Darfield (Canterbury) earthquake, New Zealand, and its impact on man-made structures, in *Ninth Pacific Conference on Earthquake Engineering, Building an Earthquake-Resilient Society,* Auckland, New Zealand, Paper 186, 8 p.

Van Dissen, R., S. Hornblow, M. Quigley, N. Litchfield, P. Villamor, and A. Nicol (2013a). Towards the development of design curves for characterising distributed strike-slip surface fault rupture displacement: an example from the 4 September, 2010, Greendale Fault rupture, New Zealand, in *19th NZGS Geotechnical Symposium*, 455-462.

Van Dissen, R., D. Rhoades, T. Little, N. Litchfield, R. Carne, and P Villamor (2013b). Conditional probability of rupture of the Wairarapa and Ōhariu faults, New Zealand. *New Zeal. J. Geol. Geophys.* **56**, 53-67.

Villamor, P., D. Barrell, N. Litchfield, R. Van Dissen, S. Hornblow, and S. Levick (2011). Greendale Fault: investigation of surface rupture characteristics for fault avoidance zonation, *GNS Science Consultency Report* 2011-121. Technical report/Environment CanterburyR11/25. 52 p.

Villamor, P., N. Litchfield, D. Barrell, R. Van Dissen, S. Hornblow, M. Quigley, S. Levick, W. Ries, B. Duffy, J. Begg, D. Townsend, T. Stahl, E. Bilderback, D. Noble, K. Furlong, and H. Grant (2012). Map of the 2010 Greendale Fault surface rupture, Canterbury, New Zealand: application to land use planning, *New Zeal. J. Geol. Geophys*. **55**, 223-230.

Wallace, L.M., J. Beavan, R. McCaffrey, K. Berryman, and P. Denys (2007). Balancing the plate motion budget in the South Island, New Zealand using GPS, geological and seismological data, *Geophys. J. Int.* **168**, 332-352.

Wang, N. (2013). *Luminescence Dating Technical Report*, no. 13/3. Luminescence dating laboratory, Victoria University of Wellingon, New Zealand.

Wells, D.L., and K.J. Coppersmith (1994). New empirical relationships among magnitude, rupture length, rupture width, rupture area, and surface displacement, *Bull. Seis. Soc. Am.* **84**, 974-1002.

Wesnousky, S.G. (2008). Displacement and Geometrical Characteristics of Earthquake Surface Ruptures: Issues and Implications for Seismic-Hazard Analysis and the Process of Earthquake Rupture, *Bull. Seis. Soc. Am.* **98,** no. 4, 1609–1632.

Wood, R.A., and R.H. Herzer (1993). The Chatham Rise, New Zealand, P. F. Ballance (ed.) *South Pacific sedimentary basins.* Amsterdam: Elsevier Science Publishers. *Sedimentary basins of the world* **2***.* 329-349.

www.gns.cri.nz

Principal Location

1 Fairway Drive
Avalon
PO Box 30368
Lower Hutt
New Zealand
T +64-4-570 1444
F +64-4-570 4600

Other Locations

Dunedin Research Centre
764 Cumberland Street
Private Bag 1930
Dunedin
New Zealand
T +64-3-477 4050
F +64-3-477 5232

Wairakei Research Centre
114 Karetoto Road
Wairakei
Private Bag 2000, Taupo
New Zealand
T +64-7-374 8211
F +64-7-374 8199

National Isotope Centre
30 Gracefield Road
PO Box 31312
Lower Hutt
New Zealand
T +64-4-570 1444
F +64-4-570 4657